| | |
|---|---|
| ***Publication Year*** | 2016 |
| ***Acceptance in OA*** | 2020-05-14T17:25:15Z |
| ***Title*** | Measuring the dynamical state of Planck SZ-selected clusters: X-ray peak - BCG offset |
| ***Authors*** | ROSSETTI, MARIACHIARA, GASTALDELLO, FABIO, Ferioli, G., Bersanelli, M., DE GRANDI, Sabrina, Eckert, D., GHIZZARDI, SIMONA, Maino, D., MOLENDI, SILVANO |
| ***Publisher's version (DOI)*** | 10.1093/mnras/stw265 |
| ***Handle*** | http://hdl.handle.net/20.500.12386/24853 |
| ***Journal*** | MONTHLY NOTICES OF THE ROYAL ASTRONOMICAL SOCIETY |
| ***Volume*** | 457 |

Monthly Notices
of the
ROYAL ASTRONOMICAL SOCIETY

MNRAS **457,** 4515–4524 (2016)
Advance Access publication 2016 February 3

doi:10.1093/mnras/stw265

# Measuring the dynamical state of *Planck* SZ-selected clusters: X-ray peak – BCG offset

M. Rossetti,[1,2★] F. Gastaldello,[2] G. Ferioli,[1] M. Bersanelli,[1] S. De Grandi,[3] D. Eckert,[2,4] S. Ghizzardi,[2] D. Maino[1] and S. Molendi[2]

[1] *Dipartimento di Fisica, Università degli Studi di Milano, via Celoria 16, I-20133 Milano, Italy*
[2] *INAF, Istituto di Astrofisica Spaziale e Fisica Cosmica, via Bassini 15, I-20133 Milano, Italy*
[3] *INAF, Osservatorio Astronomico di Brera, via E. Bianchi 46, I-23807 Merate, Italy*
[4] *Astronomy Department, University of Geneva 16, ch. d'Ecogia, CH-1290 Versoix, Switzerland*

Accepted 2016 January 29. Received 2016 January 27; in original form 2015 November 30

## ABSTRACT

We want to characterize the dynamical state of galaxy clusters detected with the Sunyaev–Zeldovich (SZ) effect by *Planck* and compare them with the dynamical state of clusters selected in X-rays survey. We analysed a representative subsample of the *Planck* SZ catalogue, containing the 132 clusters with the highest signal to noise ratio and characterize their dynamical state using as an indicator the projected offset between the peak of the X-ray emission and the position of the Brightest cluster galaxy. We compare the distribution of this indicator for the *Planck* SZ-selected sample and three X-ray-selected samples (HIFLUGCS, MACS and REXCESS). The distributions are significantly different and the fraction of relaxed objects is smaller in the *Planck* sample (52 ± 4 per cent) than in X-ray samples ($\simeq$74 per cent) We interpret this result as an indication of different selection effects affecting X-rays (e.g. 'cool core bias') and SZ surveys of galaxy clusters.

**Key words:** galaxies: clusters: general – galaxies: clusters: intracluster medium.

## 1 INTRODUCTION

In the framework of hierarchical structure formation, clusters of galaxies, the largest and most massive collapsed objects in the Universe, represent the current endpoint of the evolution of primordial density fluctuations. Thus, they are at the same time sensitive probes of the history of structure assembly and powerful tools to constrain cosmological parameters. Indeed, much effort has been devoted in recent years to exploit the cluster population for cosmological studies, complementing other methods to break degeneracies between parameters. However, the very same processes leading to the formation of clusters (i.e. accretion of smaller structures and mergers between objects with similar mass) may influence the results of cosmological studies, which often assume equilibrium and virialization, and should be properly taken into account (Planck Collaboration XX 2014; Planck Collaboration XXIV 2015).

Uncertainties in the scaling relations between observables at different wavelengths and the total mass of galaxy clusters have been shown to be the major source of systematics when using galaxy clusters as cosmological probes (e.g. Vikhlinin et al. 2009; Benson et al. 2013; Planck Collaboration XX 2014; Planck Collaboration XXIV 2015). Those uncertainties are at least partly associated with an incomplete knowledge of the physical processes affecting the baryonic components of galaxy clusters during their formation and evolution, which are not easily reproduced in cosmological simulations. Such processes are expected to play a role also in the selection of objects in clusters surveys: if they enhance (or decrease) the value of the observable used to find and select objects, the number of objects would be enhanced (or decreased) with respect to the expectation from the theoretical mass function. For instance, in X-ray surveys, the presence of a prominent surface brightness peak in the so-called 'cool core' (CC) clusters (i.e. clusters which are observationally defined by having a clear peak of X-ray emission associated with a decrease in the gas temperature, usually considered as relaxed objects) introduces a significant bias towards this class of objects (Eckert, Molendi & Paltani 2011).

Growing attention has been devoted over the last decade to an alternative method to search for galaxy clusters: the Sunyaev–Zeldovich effect (SZ, hereafter; Sunyaev & Zeldovich 1970; Sunyaev & Zeldovich 1972), i.e. the distortion of the spectrum of the cosmic microwave background (CMB) radiation induced by the Inverse Compton scattering of CMB photons on the electrons in the intracluster medium (ICM). The first large catalogues of galaxy clusters, containing hundreds of detections, have been published in recent years, using different instruments (Planck Collaboration XXIX 2014; Planck Collaboration XXVII 2015; Hasselfield et al. 2013; Bleem et al. 2015). The main advantage

---

★ E-mail: mariachiara.rossetti@unimi.it

Published by Oxford University Press on behalf of the Royal Astronomical Society

of SZ surveys is that the SZ spectral distortion does not depend on the redshift of the source, allowing us to construct virtually mass-limited samples and to eventually detect all massive clusters in the Universe, irrespective of their distance. Moreover, SZ quantities do not depend much on the details of the cluster physics and on the dynamical state of the cluster (Motl et al. 2005; Battaglia et al. 2012; Krause et al. 2012). Recently, Planck Collaboration XXVII (2015) used Monte Carlo simulations to show that the cluster morphology has a negligible impact on the source detection procedure in the *Planck* survey. However, according to simulations (Pipino & Pierpaoli 2010; Lin et al. 2015), the presence of a peaked pressure profile in CC clusters results in an increase in the central value of the Comptonization parameter,[1] which could induce a bias in favour of cool cores (CCS) also in SZ surveys. This effect is nonetheless expected to be small, especially for an instrument like *Planck* whose spatial resolution is larger than the typical size of the cores of galaxy clusters and is thus more sensitive to the integrated total SZ signal rather than to its central value (Pipino & Pierpaoli 2010; Lin et al. 2015).

On the observational side, only limited information is available yet on the properties of SZ-selected clusters, including their dynamical state. The majority of objects newly discovered by *Planck* show clear indication of morphological disturbances in their X-ray images, suggesting an active dynamical state (Planck Collaboration IX 2011), but a statistical analysis on the whole sample (or on a representative subsample) is necessary to draw any conclusion. For this reason, we performed the analysis described in the present paper which aims at measuring for the first time the dynamical state of a representative sample of *Planck* SZ-selected clusters through an indicator of dynamical activity and compare it with the corresponding distribution for X-ray-selected samples to answer to the following question: is the cluster population selected through the SZ effect different, in terms of dynamical state, than the X-ray-selected population?

'Measuring' the dynamical state of a cluster is not an easy task. In principle, the maximum amount of information on the dynamical history of a cluster can be derived by a detailed spatially-resolved two-dimensional mapping of thermodynamic quantities, of metal abundance distribution, associated with the study of the galaxy population, eventually to the presence of diffuse radio sources (haloes and/or relics) and possibly to the mass distribution through gravitational lensing. However, this wealth of information is available only for a very limited number of objects and moreover it cannot be easily quantified in a single dynamical indicator. The X-ray band alone can be successfully used to derive information on the dynamical activity, since merger events leave strong signatures in the thermodynamic quantities and morphological appearance of the ICM. Powerful indicators assess the presence or absence of a CC, such as central entropy (Cavagnolo et al. 2009), pseudo-entropy ratio (Leccardi, Rossetti & Molendi 2010) or cooling time (Peres et al. 1998), but require spectroscopic analysis and eventually deprojection. Less expensive indicators of dynamical activity can be computed basing only on the morphology of X-ray images, such as power ratios (Buote & Tsai 1995), centroid shifts (Poole et al. 2006) and the concentration parameter (Santos et al. 2008). An alternative approach to quantify the dynamical state can be built on the different physical processes undergone by the collisional ICM and the collisionless galaxy population during cluster mergers. In particular, brightest cluster galaxies (BCGs) are of particular interest as they represent a unique class of objects (e.g. Lauer et al. 2014). They are the most massive and luminous galaxies in the Universe and their properties are found to correlate with many global cluster properties such as X-ray temperature or luminosity (e.g. Edge 1991; Edge & Stewart 1991; Brough et al. 2005, 2008) indicating that their origin is closely related to that of the host cluster. If clusters are dynamically relaxed systems, we naturally expect the BCG to be at rest at the centre of the gravitational potential well, an assumption referred to as the 'central galaxy paradigm' (van den Bosch et al. 2005; Cui et al. 2016). However since the first X-ray images of clusters with the *Einstein* satellite became available, it became clear that there is a class of clusters for which BCGs are not close to the X-ray centres of their host clusters (Jones & Forman 1984, 1999). The X-ray studies complemented and supported the early evidence coming from the optical band that BCGs may not always be at the centre of the galaxy surface distribution (e.g. Beers & Geller 1983) and velocity space (e.g. Malumuth et al. 1992; Oegerle & Hill 2001). The connection between the presence of offsets and the disturbed dynamical state of the cluster due to a merger has been progressively established in observational studies (Katayama et al. 2003; Patel et al. 2006) and simulations (e.g. Skibba & Macciò 2011). With the current generation of X-ray satellites, *Chandra* and *XMM–Newton*, it has become possible to strengthen the correlation between the X-ray peak-BCG offset and a disturbed dynamical state (such as lack of a CC and disturbed X-ray morphology; Sanderson, Edge & Smith 2009; Hudson et al. 2010; Mann & Ebeling 2012; Hashimoto, Henry & Boehringer 2014) and to establish this indicator as a simple but robust diagnostic of an active dynamical state. Sometimes the different flavour of using the X-ray centroid rather than peak is used, but leading to basically the same results (Mann & Ebeling 2012).

In this paper, we measure the offset between the X-ray peak and the BCG population as indicator of dynamical state of *Planck* SZ-selected clusters and compare its distribution to the one of X-ray-selected samples to provide a first answer to the question we posed above. Therefore we can re-formulate the aforementioned question as: is the distribution of the BCG-X-ray peak offset in the *Planck* SZ survey different than in X-ray-selected samples? This question is obviously less ambitious than our starting question but it represents a first significant step towards a more complete characterization of the population of clusters selected through the SZ effect.

In this paper, we assume Λ-CDM cosmology with $H_0 = 70\,\mathrm{km\,s^{-1}\,Mpc^{-1}}$, $\Omega_\mathrm{m} = 0.3$ and $\Omega_\Lambda = 0.7$. The outline of the paper is as follows: in Section 2, we introduce our sample and describe the procedure we used to measure our indicator. In Section 3.1, we describe the distribution of the BCG-X-ray peak offset in the *Planck* sample and compare it to X-ray-selected samples in Section 3.2. We discuss our findings and provide an interpretation in Section 4.

## 2 DATA ANALYSIS

### 2.1 The sample

The starting point of our analysis is the *Planck* cosmology sample (PSZ1-cosmo) described in Planck Collaboration XX (2014). It is a high-purity subsample constructed from the first release of the *Planck* catalogue of SZ sources (Planck Collaboration XXIX 2014), by imposing a signal-to-noise ratio (S/N) threshold of 7 and applying a mask, that excludes the galactic plane and point sources leaving 65 per cent of the sky for the survey. It contains 189 bona fide clusters with associated redshifts and has been used for

---

[1] We recall that the dimensionless Comptonization parameter, $y$, is proportional to the integral of the ICM pressure along the line of sight.

the cosmological analysis with cluster number counts described in Planck Collaboration XX (2014). The first release of the *Planck* SZ catalogue (PSZ1, hereafter) has benefited from a massive multi-wavelength follow-up campaign to confirm the detected candidates, measure their redshifts and characterize the sample. More specifically the cosmology sample has been almost completely followed-up in X-rays with either *Chandra* or *XMM–Newton* allowing us to have a reliable estimate of the peak position (see Section 2.2). Since a similar campaign has not been possible yet for the larger and more recent second release of the *Planck* SZ catalogue (PSZ2, Planck Collaboration XXVII 2015), we decided to base our analysis on the PSZ1 catalogue.

Unfortunately, we do not have literature information concerning the BCGs of all the clusters in the PSZ1 cosmological sample (Section 2.3) and not all the X-ray observations are public yet. In order to minimize the number of clusters lacking the offset measurement, we decided to extract a subsample from the PSZ1-cosmo, by imposing S/N > 8. We decided to cut in signal to noise to reproduce as closely as possible the selection function of *Planck* SZ surveys. With such more stringent S/N threshold, our final sample is composed of 136 objects: except for four objects lacking X-ray observations (Section 2.2), we could measure the BCG-peak offset for the remaining 132 clusters. We verified that our sample is representative of the parent PSZ1-cosmo sample by performing a Kolmogorov–Smirnov (KS) test on their distributions of redshifts (probability that they are drawn from the same parent distribution $p_0 = 0.97$) and masses ($p_0 = 0.82$).

We provide the list of clusters in our sample in Table 1, where we list the index and name in the PSZ1 catalogue, the redshift and the angular size $\Theta_{500}$, corresponding to $R_{500}$. We estimated this latter quantity using the redshift and masses in the updated PSZ1 catalogue (Planck Collaboration XXXII 2015), which were obtained with the *Y–M* scaling relation in Planck Collaboration XX (2014).

## 2.2 Determining the X-ray peak

We determined the coordinates of the X-ray peak using X-ray images obtained with the current generation high-spatial resolution X-ray telescopes, preferentially *Chandra*. We downloaded the *Chandra* raw images[2] of 125 clusters from the archive and visually inspected them to identify bright point sources We smoothed the images with a Gaussian function with full width at half-maximum (FWHM) = 3–5 pixels and mark the position of the brightest pixels (excluding point sources). Seven clusters in our sample were not observed with *Chandra* but had public *XMM–Newton* observations, that we used to estimate the peak position. We could not determine the position of the X-ray peak for four clusters in our reduced *Planck* sample of 136 objects which have been observed by *Chandra* but whose observations are not public yet. The absence of this very small number of clusters from our sample does not introduce any

**Table 1.** Properties of the clusters in our sample. Column [1] is the INDEX in the PSZ1 catalogue, column [2] the *Planck* name, column [3] provides an alternative name and column [4] the redshift of the cluster. Columns [5] and [6] are the coordinates of the X-ray peak, while Columns [7] and [8] are the coordinates of the BCG and Column [9] the reference we used to associate a BCG to each cluster. Column [10] is the angular scale corresponding to $R_{500}$ and Columns [11]–[13] provide our indicator $D_{\rm X\text{–}BCG}$ in units of arcsec, kpc and $0.01R_{500}$.

| INDEX | NAME | Alt. name | $z$ | $\mathrm{RA_X}$ | $\mathrm{Dec._X}$ | $\mathrm{RA_{BCG}}$ | $\mathrm{Dec._{BCG}}$ | Reference BCG | $\Theta_{500}$ (arcmin) | (arcsec) | $D_{\rm X,\,BCG}$ (kpc) | $0.01R_{500}$ |
|---|---|---|---|---|---|---|---|---|---|---|---|---|
| 10 | PSZ1 G003.93−59.42 | RXC J2234.5−3744 | 0.151 | 338.6166 | − 37.7297 | 338.61 | − 37.744 | Coziol et al. (2009) | 8.02 | 54.70 | 143.8 | 11.37 |
| 17 | PSZ1 G006.45+50.56 | RXC J1510.9+0543 | 0.0766 | 227.7339 | 5.7446 | 227.734 | 5.745 | Coziol et al. (2009) | 15.00 | 1.56 | 2.3 | 0.17 |
| 18 | PSZ1 G006.68-35.52 | RXC J2034.7−3548 | 0.0894 | 308.6865 | − 35.8162 | 308.689 | − 35.824 | Coziol et al. (2009) | 10.93 | 29.02 | 48.4 | 4.42 |
| 23 | PSZ1 G008.33−64.74 | ACO S 1077 | 0.312 | 344.7013 | − 34.8023 | 344.7016 | − 34.8022 | Stanford et al. (2002) | 4.58 | 0.86 | 3.9 | 0.31 |
| 24 | PSZ1 G008.42−56.34 | RXC J2217.7−3543 | 0.1486 | 334.4407 | − 35.7243 | 334.441 | − 35.725 | Coziol et al. (2009) | 7.32 | 2.78 | 7.2 | 0.63 |
| 26 | PSZ1 G009.02−81.22 | RXC J0014.3−3023 | 0.3066 | 3.5814 | − 30.3917 | 3.5864 | − 30.391 | Owers et al. (2011) | 4.97 | 15.90 | 71.9 | 5.33 |
| 54 | PSZ1 G021.10+33.24 | RXC J1632.7+0534 | 0.1514 | 248.1955 | 5.5758 | 248.1958 | 5.5757 | Zhang et al. (2011) | 8.49 | 1.08 | 2.8 | 0.21 |
| 76 | PSZ1 G029.10+44.54 | RXC J1602.3+1601 | 0.0353 | 240.5709 | 15.9745 | 240.571 | 15.9747 | Hoffer et al. (2012) | 23.73 | 0.45 | 0.3 | 0.03 |
| 92 | PSZ1 G033.43−48.44 | RXC J2152.4−1933 | 0.0943 | 328.0882 | − 19.5478 | 328.0915 | − 19.5468 | Hoffer et al. (2012) | 10.45 | 11.46 | 20.1 | 1.83 |
| 93 | PSZ1 G033.84+77.17 | RXC J1348.8+2635 | 0.0622 | 207.22 | 26.5899 | 207.219 | 26.593 | Coziol et al. (2009) | 15.94 | 11.71 | 14.0 | 1.22 |

---

[2] The images available in the *Chandra* archive are not exposure corrected. We verified ‘a posteriori’ our method of finding the peak position by comparing our estimate with the one provided in Hudson et al. (2010) for HIFLUGCS (Section 3.2). The median difference is 3 kpc and large separation are found only for very few clusters featuring a rather uniform brightness distribution, where the choice of the brightest pixel may be affected by small exposure corrections as well as statistical fluctuations. We do not expect this effect to induce a significant systematic bias in our measurements of the offset between the X-ray peak and the BCG position, since these effects are not related to the BCG position.

foreseeable bias, as these four objects are not peculiar in terms of redshift and mass and they are not new *Planck* discovered objects.

In principle, the superb angular resolution of *Chandra* allows us to estimate the position of the peak of the X-ray emission with great accuracy, <0.3 arcsec (Evans et al. 2010), which at the median redshift of our sample corresponds to <8 kpc. However, as discussed in Mann & Ebeling (2012), the accuracy on the position also depends on the statistical quality of the observations, on the possible presence of non-detected point sources and on the surface brightness distribution (i.e. presence of multiple peaks). It is thus not easy to estimate this uncertainty for all clusters and the astrometric error reported above should be considered only a lower limit. Moreover, in seven cases, we could not use *Chandra* observations but used the lower resolution *XMM–Newton* data which are characterized by a larger positional error: we verified a posteriori that the use of these instruments does not affect our conclusions by excluding them from our sample and finding consistent results. However, the uncertainty in the positional reconstruction is not a systematic error, as it will not produce systematically larger or smaller offsets. Indeed, in the few cases where two possible peaks were detected (as for instance in double systems or in the presence of infalling subclusters) we always chose the brightest pixel, regardless of its proximity to the BCG.

### 2.3 Finding the BCG

We based our search for BCGs mainly on literature information: optical catalogues of galaxy clusters which provide the position of the BCG (MaxBCG, Koester et al. 2007; Wen12, Wen, Han & Liu 2012; redMaPPer,[3] Rykoff et al. 2014) and papers providing the position of the BCGs for different samples of galaxy clusters (Coziol et al. 2009; Hoffer et al. 2012; Crawford et al. 1999; Zhang et al. 2011; Mann & Ebeling 2012; Song et al. 2012; Menanteau et al. 2010). We first cross matched our sample with the BCG catalogues listed above using TOPCAT (Taylor 2005) and associated a BCG to 98 clusters. We evaluated case by case the objects where two different BCGs were associated by different catalogues to the same cluster (the most relevant examples are provided in Appendix A) and we selected as BCG the brightest one in the NASA/IPAC Extragalactic Database[5] data base.

For 38 objects, we could not find any information in the catalogues and papers listed above. We thus searched in NED for galaxies around the X-ray position in a circle with radius $R_{500}$. In 18 cases, one of the galaxies (the brightest in the list) was cited as BCG in one or more literature works (optical studies of individual objects or BCG catalogues for smaller sample of clusters). We associated those BCGs to their clusters and refer to the papers who made that association in Table 1.

For the remaining 16 clusters, which are all out of the sky region covered by the Sloan Digital Sky Survey (SDSS), we made our own choice of the BCG as the brightest source (using 2MASS magnitudes) classified as galaxy and with a redshift consistent with that of the source in the objects found by the NED data base within $R_{500}$ of each cluster. We then visually inspected the Digitized Sky Survey (DSS) images of those clusters to confirm the identification of the BCGs.

We could associate a BCG to all clusters in our sample and therefore measure the projected offset between the BCG and the X-ray peak ($D_{\rm X-BCG}$ hereafter) for 132 clusters. In Table 1, we provide the coordinates of the BCG and the X-ray peak as well as our measured $D_{\rm X-BCG}$ in arcsec, kpc and fractions of $R_{500}$.

The optical information from which we derived the positions of the BCGs is very heterogeneous and it is thus difficult to estimate the uncertainties in our measurements. First of all, different data sets have different absolute astrometric accuracy. Secondly, different choices and methods (optical selection, searching radius, colours) made by the authors of the references we used, introduce an uncertainty in our data which is likely dominant over the error on the galaxy position. In a few cases, some of the literature work we have used for BCG association may have induced a systematic bias in our analysis by limiting the BCG search in a radius smaller than $R_{500}$ (e.g. Hoffer et al. 2012 search the BCG in a 5 arcmin × 5 arcmin field of view centred on the X-ray position, which is often smaller than a circle with radius $R_{500}$ for low-redshift systems) or by choosing the BCG closer to the X-ray peak in systems with two or more galaxies with comparable magnitudes. Therefore, it is possible that in a few cases our offsets may be underestimated.

## 3 RESULTS

### 3.1 The offset distribution of the *Planck* sample

As described in Section 2, we could measure the offset between the peak of the X-ray emission and the BCG position for our sample of 132 *Planck*-selected clusters. In Fig. 1, we show the distribution of our indicator $D_{\rm X-BCG}$ both in units of kpc and rescaled by $R_{500}$. The shape of the distribution is roughly lognormal, with a median value $0.017R_{500}$ (21.5 kpc) and has a large spread which can be expressed in terms of the Interquartile Range[6] (IQR $= 0.066R_{500}$ or 82.4 kpc). When plotted in logarithmic scale, the distribution is not symmetric around the maximum but skewed towards large offset values. Indeed, a significant number of objects feature separations of the order of hundreds of kpc and of large fractions of $R_{500}$.

The distribution in Fig. 1 is not bimodal and does not provide us a clear threshold to divide clusters in two separate classes, ‘relaxed’ and ‘disturbed’. In the literature, Mann & Ebeling (2012) classify objects with an offset >42 kpc as ‘extreme mergers’ and 50 clusters in our sample (38 per cent of the total) would fall in this class. However, given the relatively large mass range in our sample (covering about an order of magnitude) and since we want to compare it with other samples (Section 3.2), we prefer to define a more physically interesting threshold in terms of $R_{500}$. Sanderson et al. (2009) divide their objects into two classes: ‘small offset’ ($<0.02R_{500}$) systems, which can be considered as relaxed, and ‘large offset’ ($>0.02R_{500}$) systems which are likely disturbed. We decided to follow this convention, and in the rest of this paper, we define as ‘relaxed’ the 68 objects where the offset is smaller than $0.02R_{500}$. We thus find a fraction of relaxed object in our sample of $(52 \pm 4)$ per cent, where we estimated the error with bootstrap resampling.

---

[3] In the redMaPPer algorithm the centring of the clusters is fully probabilistic, to take into account multiple candidate central galaxies. We thus verified one by one the associations with redMaPPer clusters.

[5] https://ned.ipac.caltech.edu/

[6] The IQR is an indicator of the statistical dispersion of a distribution and is defined as the difference between the third (75th percentile) and the first (25th percentile) quartiles.

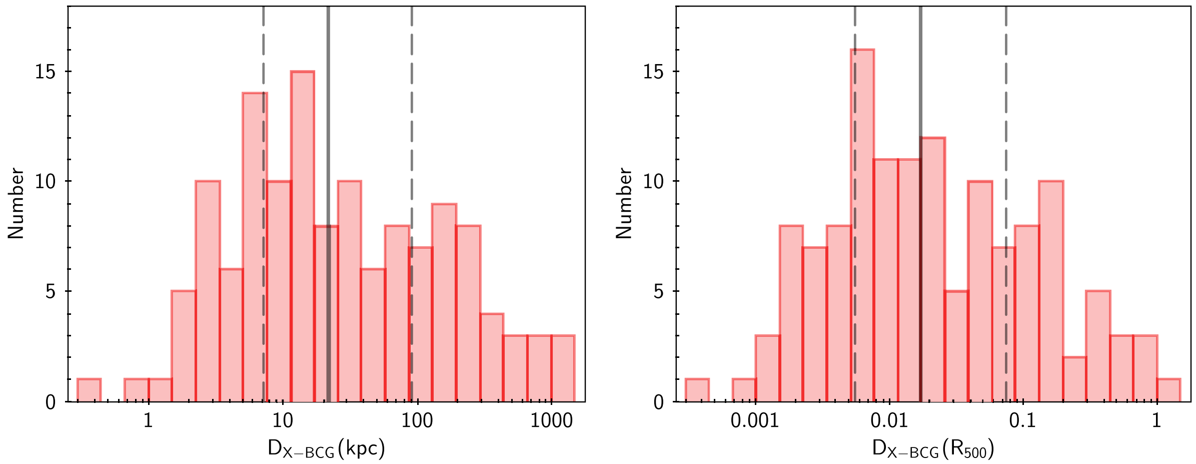

**Figure 1.** Offset distribution between the X-ray peak and the BCG position in units of kpc (left) and $R_{500}$ (right) for our *Planck* sample. The grey line indicates the median of the distributions and the dashed lines the first and the third quartiles.

We divided our sample into two halves, first a 'low-redshift' and a 'high-redshift' subsamples (splitting around the median value $z = 0.16$) then a 'low-mass' and a 'high-mass' subsamples (around the median value $M_{500} = 6.4 \times 10^{14}\,\mathrm{M}_{\odot}$). We compare the offset distributions in units of $R_{500}$ for the different subsamples. We calculated for each subsample the fraction of relaxed objects and found 64 per cent for the low-$z$ and 39 per cent for the high-$z$, 62 per cent for the low mass and 41 per cent for the high mass, with an uncertainty of 6 per cent in each subsample. The difference in the relaxed fraction between low-$z$ and high-$z$ is significant at $2.8\sigma$ and provides some indication of an evolution with redshift. We observe a slightly less significant, but still tantalizing, difference ($2.5\sigma$) between the low-mass and high-mass subsamples. We may furthermore compare the subsamples by trying to assess the probability that they are drawn from the same parent distribution. This is a classical problem in statistics and since we do not know the underlying distribution we resort to non-parametric test. We follow the advice of Wall & Jenkins (2003) (see their table 5.6) and choose the most efficient non-parametric tests: the KS two-sample test and the Wilcoxon–Mann–Withney (WMW) *U*-test. The KS test in its two-tailed version applied in this study is sensitive to any form of difference between the two distributions. The *U*-test is sensitive to the position of the distributions, i.e. location of means and medians. We follow the suggestion of Feigelson & Babu (2012) and compare the results of more than one method, as various tests have different efficiencies under various conditions. We apply the above tests using the R environment for statistical computing (R Core Team 2015) and we show our results are in the upper part of Table 2: we find significant indication (null-hypothesis probability $p_0 < 0.2$ per cent) that the distribution is different in the two redshift subsamples and some indication ($p_0 < 4$ per cent) in the two mass bins. Given the limited number of objects in our sample, especially at high redshifts and mass, we cannot divide our sample in more mass and redshift bins, otherwise we would be dominated by statistical uncertainty. Moreover, there is a significant overlap between our low-redshift and low-mass subsamples, as well as in the high mass and high $z$, because the least massive objects are detected only locally in the *Planck* survey (see the distribution of objects in the mass–redshift plane in the PSZ1 Planck Collaboration XXIX 2014). Therefore it is not possible to assess if we are observing a dependence of the relaxed fraction on the mass, redshift or both.

**Table 2.** Results of statistical tests comparing two distributions: we provide the statistic *D* of the Kolmogorov–Smirnov test and *U* of the Wilcoxon–Mann–Withney, as well as the null-hypothesis probability $p_0$ in both cases. The first two lines refer to the comparison between redshift and mass subsamples of the *Planck* sample (Section 3.1). The middle lines refer to the comparison between our *Planck* samples and the X-ray-selected samples (Section 3.2). The bottom lines compare only the high-redshift and high-mass subsamples of *Planck* and MACS to assess the origin of our results (Section 4.1).

| Compared samples | KS test | | WMW test | |
|---|---|---|---|---|
| | $D$ | $p_0$ | $U$ | $p_0$ |
| *Planck* redshift bins | 0.323 | $2.1\,10^{-3}$ | 2823 | $9.5\,10^{-4}$ |
| *Planck* mass bins | 0.246 | $3.8\,10^{-2}$ | 2555 | $3.9\,10^{-2}$ |
| *Planck*–HIFLUGCS | 0.336 | $1.1\,10^{-4}$ | 5440 | $5.6\,10^{-5}$ |
| *Planck*–MACS | 0.228 | $4.2\,10^{-3}$ | 8865 | $4.4\,10^{-4}$ |
| *Planck*–REXCESS | 0.297 | $2.2\,10^{-2}$ | 2637 | $3.9\,10^{-2}$ |
| *Planck*–MACS high-$z$ | 0.375 | $1.6\,10^{-5}$ | 4903 | $8.7\,10^{-7}$ |
| *Planck*–MACS high-$M$ | 0.336 | $1.2\,10^{-3}$ | 2720 | $1.4\,10^{-4}$ |

### 3.2 Comparison with X-ray-selected samples

In order to answer the question we asked in Section 1, we need to compare the offset distribution that we obtained for our sample with a consistent distribution for X-ray-selected samples. The offset distribution has been studied in the literature by many authors for several samples of galaxy clusters (Lin & Mohr 2004; Sanderson et al. 2009; Haarsma et al. 2010; Zhang et al. 2011; Mann & Ebeling 2012; Stott et al. 2012). However, since we want to compare the offset distribution of SZ selected clusters with X-ray-selected clusters, we compare our distribution only with the samples that ensure rigorous selection criteria based on X-ray surveys. Moreover, as shown in 3.1, the $D_{\mathrm{X,\,BCG}}$ distribution may evolve with redshift and mass, so ideally we would like to compare our *Planck* sample with an X-ray-selected sample with the same redshift and mass distribution. However, such a sample does not exist because of the different selection functions in the mass–redshift plane of SZ and X-ray surveys. Therefore we decided to compare our sample with three X-ray-selected samples, with different mass and redshift ranges (Fig. 2), which are described below.

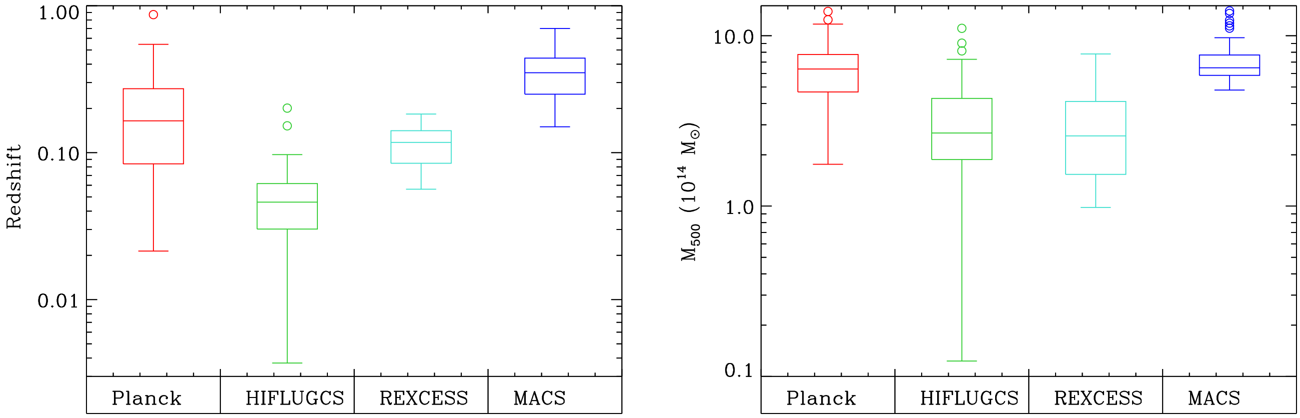

**Figure 2.** Box-and-Whiskers plot representing the redshift (left) and mass (right) distribution of the *Planck* sample compared to the three X-ray-selected samples. The empty circles mark outliers in the distribution, selected for being values larger than the 75th percentile +1.5IQR. The properties of the *Planck* sample are intermediate between the low-redshift, low-mass objects of the HIFLUGCS and REXCESS sample and the high-mass, high-$z$ distribution of MACS.

(i) *HIFLUGCS* (The HIghest X-ray FLUx Galaxy Cluster Sample; Reiprich & Böhringer 2002) is a complete flux-limited sample, comprising the 64 X-ray brightest clusters ($F_X$[0.1−2.4 keV)] > 2 $10^{-11}$ erg $s^{-1}$ $cm^{-2}$) outside of the galactic plane. The position of their BCGs is reported in Zhang et al. (2011), who base their analysis on optical data obtained within an aperture >2.5 Mpc, larger than the typical $R_{500}$ of their clusters. As Zhang et al. (2011) measure their offset from the X-ray centroid not from the X-ray peak, we estimated the position of the X-ray peak also for the HIFLUGCS clusters using the procedure described in Section 2.2[7] and we used them to measure $D_{\rm X,\,BCG}$, that we normalized using their $R_{500}$ estimate. The offset distribution shown in the left-hand column of Fig. 3 has a median value 3.8 $10^{-3}$ and IQR 1.8 $10^{-2}$.

(ii) REXCESS (The REpresentative XMM-Newton Cluster Structure Survey; Böhringer et al. 2007) is a representative and statistically unbiased subsample of 33 galaxy clusters extracted from the *REFLEX* cluster catalogue with a rigorous selection in the luminosity–redshift space (see details in Böhringer et al. 2007). The BCG coordinates, the offset from the X-ray peak and $R_{500}$ have been published by Haarsma et al. (2010) for 30 objects. The BCG is estimated basing on optical data obtained with instruments with field of view about 5–7 arcmin across, which can be smaller than $R_{500}$ of the clusters for a large part of the sample. It is thus possible that some of the offsets may be underestimated. The $D_{\rm X,\,BCG}$ distribution shown in the middle column of Fig. 3 has a median value 7.9 $10^{-3}$ and IQR 1.0 $10^{-2}$.

(iii) MACS (The MAssive Cluster Survey; Ebeling, Edge & Henry 2001) is a survey to find the most massive clusters at high redshift $z > 0.3$ starting from the ROSAT All Sky Survey catalogue and using optical data to confirm cluster candidates. The offset between the X-ray peak and the BCG has been measured by Mann & Ebeling (2012) for a subsample of 108 objects, starting from a flux threshold ($F_X$[0.1−2.4 keV] > $10^{-12}$ erg $s^{-1}$$cm^{-2}$) with additional luminosity and redshift criteria ($L_X$[0.1−2.4 keV] > 5 $10^{44}$ erg $s^{-1}$ and $z > 0.15$). Since the authors do not provide the $R_{500}$ values for their clusters but provide the X-ray luminosity, we estimated $M_{500}$ and $R_{500}$ using the $L$–$M$ scaling relation by Arnaud et al. (2010). The BCG is estimated for 77 clusters basing on imaging data from the UH2.2 m telescope, with a field of view of 7.5 arcmin × 7.5 arcmin, which is larger than the $R_{500}$ region for the majority of these clusters, but not for all of them. For the remaining clusters, the BCG was estimated basing on SDSS or DSS data but the searching radius is not specified. It is thus possible that some of the offsets may be underestimated. The $D_{\rm X,\,BCG}$ distribution shown in the right-hand column of Fig. 3 has a median value 8.7 $10^{-3}$ and IQR 1.7 $10^{-2}$.

As shown in Fig. 2, the three X-ray samples feature different redshift and mass distributions. While HIFLUGCS is composed mainly of local and relatively low-mass objects, MACS by construction contains massive systems at high redshift. REXCESS contains objects at intermediate redshift, with median mass similar to HIFLUGCS.

In Fig. 3, we compare the distribution of $D_{\rm X,\,BCG}$ in units of $R_{500}$ of our *Planck* sample with the three X-ray samples described above, and show the normalized histogram, and the cumulative distribution. In all cases, we note that the *Planck* distribution is skewed towards larger offset than the X-ray ones and that the *Planck* cumulative distribution rises less steeply than for the X-ray samples. The visual impression that the distributions are different, is supported also by the differences in the medians (0.017 versus 4–8 $10^{-3}$ $R_{500}$) and IQR (0.066 versus 0.01–0.04 $R_{500}$).

We applied the same statistical tests as in Section 3.1 to assess the probability that each of the X-ray-selected samples may be drawn from the same parent distribution of our *Planck* sample and we report the results in Table 2. The significance of the results depends on the test applied and on the samples: the null-hypothesis probability is always <0.4 per cent for the MACS and HIFLUGCS sample and of the order of 2–4 per cent for the smaller REXCESS sample. We can thus conclude with a high reliability that the offset distribution in the *Planck* sample is different than in the X-ray-selected samples.

One possible concern in comparing the normalized distributions of the *Planck* and X-ray samples is a possible difference in the $R_{500}$ estimate. To test this, we compared the $R_{500}$ values for clusters in common with the *Planck* sample (28 objects in HIFLUGCS, 7 in REXCESS and 32 in MACS). The points show a ∼10 per cent scatter around the equality line, which likely reflects the scatter in the parent scaling relations used to estimate $R_{500}$, and a small systematic offset, with *Planck* $R_{500}$ values being on average larger by 3 per cent than $R_{500}$ values in X-ray samples. This means that offsets in the *Planck* sample are on average slightly smaller than the offsets in X-ray samples for common clusters. Correcting for this

---

[7] We later realized that the positions of the peaks for the HIFLUGCS clusters were provided by Hudson et al. (2010). We found a good agreement between the estimates with a median separation of 3 kpc.

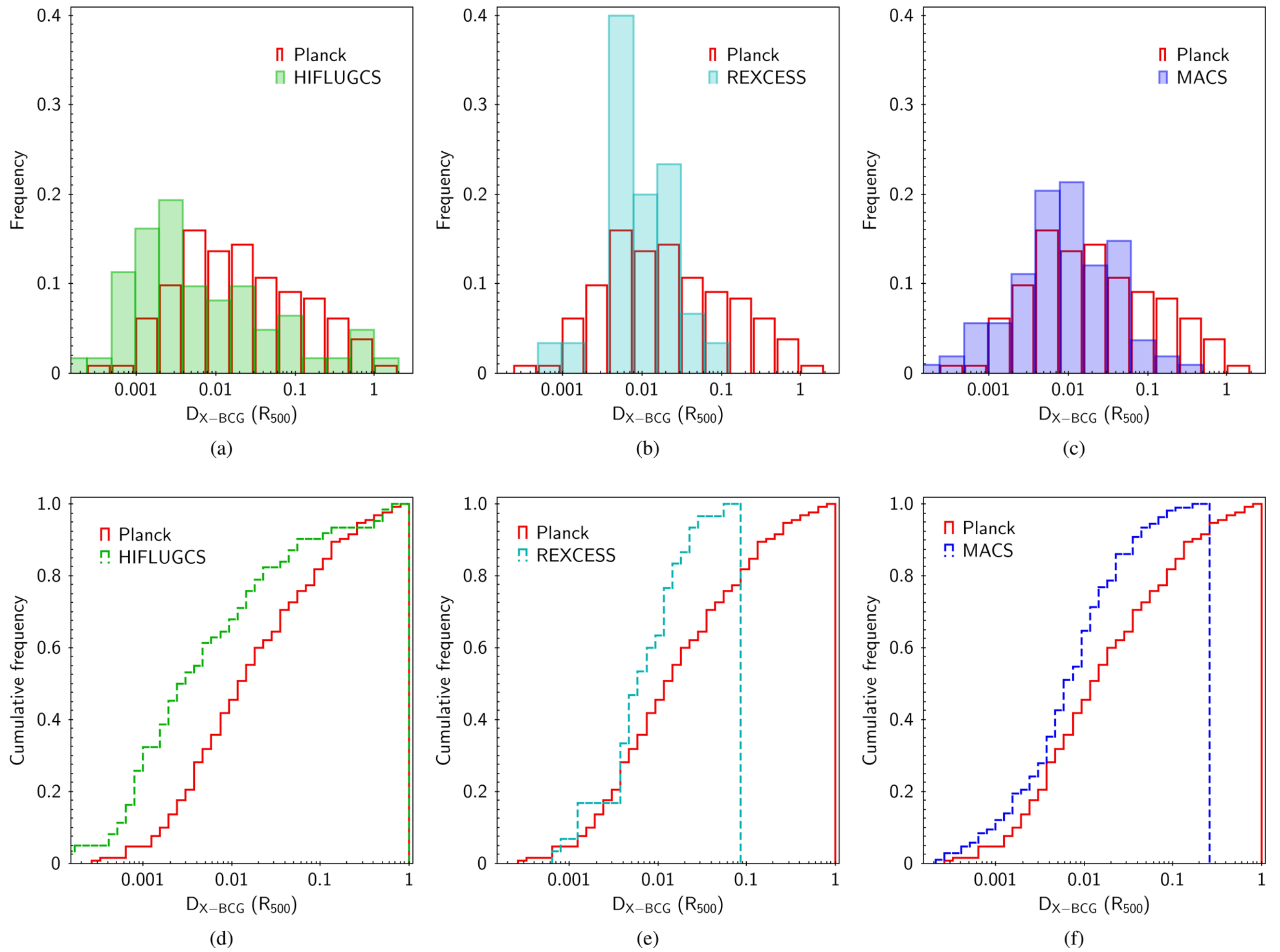

(a) (b) (c)

(d) (e) (f)

**Figure 3.** Distribution of the offset between the X-ray peak and the BCG for the *Planck* sample (red empty histogram and solid line) compared with HIFLUGCS (left, green filled histogram and dashed line), REXCESS (middle, cyan filled histogram and dashed line) and MACS (right, blue filled histogram and dashed line). In the top row, we show the normalized histograms and in the bottom row, the cumulative distribution.

small systematic effect would thus lead to larger offsets in *Planck* clusters, making the SZ offset distribution even more different with respect to the X-ray ones and therefore a systematic bias in the $R_{500}$ estimate cannot be used to explain the discrepancy we found.

Following our classification scheme ($D_{\rm X,\,BCG} < 0.02R_{500}$, Section 3.1), we calculated the fraction of relaxed objects to be (74 ± 5) per cent in HIFLUGCS (73 ± 4) per cent in MACS and (77 ± 7) per cent in REXCESS, while it is only (52 ± 4) per cent in our sample. We computed with a Monte Carlo simulation the probability of obtaining randomly from the *Planck* sample the fraction of relaxed clusters of X-ray samples and found 0.05 per cent for *HIFLUGCS*, <0.001 per cent for MACS, 0.2 per cent for REXCESS. We conclude that the fraction of relaxed objects is significantly larger in X-ray samples than in the *Planck* SZ-selected sample.

## 4 DISCUSSION

### 4.1 SZ versus X-ray selection

The analysis of the distribution of $D_{\rm X,\,BCG}$ and the comparison with X-ray-selected samples shown in Section 3, allow us to address the question we asked in Section 1. Indeed, we can answer that the distribution of our indicator is significantly different in the *Planck* sample with respect to all X-ray-selected samples we considered. The significance of this result can be assessed both with statistical tests on the whole distributions and on the fraction of relaxed clusters. In the former test, the null hypothesis probability that the *Planck* sample and each of the X-ray-selected samples are drawn from the same parent distribution is always <0.4 per cent (depending on the test) for MACS and HIFLUGCS and of the order of 2–4 per cent for the smaller REXCESS sample. In the latter comparison, the fraction of relaxed objects in the *Planck* sample (52 ± 4 per cent) differs at more than 3$\sigma$ from the fraction in X-ray-selected samples (3.4$\sigma$ HIFLUGCS, 3.7$\sigma$ MACS and 3.1$\sigma$ REXCESS, where $\sigma$ is the combined uncertainty obtained by adding in quadrature the errors in each data set). Therefore, we can answer that, according to our indicator $D_{\rm X,\,BCG}$, the dynamical state of *Planck* SZ-selected clusters is significantly different from X-ray-selected samples.

We now address the origin of this result, which may be due either to different selection effects in SZ versus X-ray surveys or to a different mass and redshift distribution in the *Planck* and in X-ray samples (Section 3.1). The three X-ray-selected samples we considered feature different properties, reflecting their selection functions: while HIFLUGCS is mainly composed of local and relatively low-mass systems, clusters in MACS are massive systems at $z > 0.1$ and the REXCESS sample shows intermediate properties. *Planck* clusters are mainly massive objects (2–20 $10^{14}$ $\rm M_{\odot}$) with a broad redshift distribution. The fact that we find similar results when comparing the *Planck* sample both with a local low-mass sample as HIFLUGCS and with a high-mass, high−z sample as MACS suggests that the differences we found are likely not due to the different mass and redshift distributions, but rather to different selection effects. To make a further test, we compared our high-$z$ and high-mass *Planck* subsample (Section 3.1) with subsamples extracted from the MACS sample with the same criteria ($z > 0.16$, basically the whole MACS, and $M_{500} > 6.4 \times 10^{14}\,\mathrm{M}_{\odot}$) and we applied the KS and WMW–$U$ tests. We still find significant differences, with null-hypothesis probabilities $p_0 < 1$ per cent (Table 2) suggesting that a large part of the discrepancy is due to the selection method.

It is well known that X-ray selection is biased towards relaxed clusters with a centrally peaked surface brightness profile(‘cool core’ clusters, or CC): Eckert et al. (2011) estimate that the fraction of strong CC clusters in HIFLUGCS is overestimated by 29 per cent, correct for this bias and predict this fraction to be in the range of 35–37 per cent. While the fraction of CC objects slightly depends on the indicator used to classify clusters, the fraction reported above is much lower than the value reported for most X-ray-selected samples. The offset between the X-ray peak and the BCG is not a direct indicator of a CC, although it has been shown to correlate well with the core state (Sanderson et al. 2009) and we cannot use it to make a direct comparison between our fraction of relaxed objects and the CC fraction reported above. However, Eckert et al. (2011) provided an ‘unbiased’ subsample of HIFLUGCS, which should be free of the CC bias, and we could estimate the fraction of relaxed objects in this subsample using the offsets measured by Zhang et al. (2011). We found a relaxed fraction of 68 ± 7 per cent in the HIFLUGCS-unbiased subsample, which is smaller than in the full HIFLUGCS sample but still significantly larger that the value in the *Planck* sample. This residual discrepancy may results from several factors. First of all, the HIFLUGCS-unbiased subsample is not complete, as it was built as a subset of the HIFLUGCS sample and not of the parent RASS data (see discussion in Eckert et al. 2011). More importantly, HIFLUGCS and its unbiased subsample have a very different mass and redshift distribution (Fig. 2) with respect to the *Planck* sample, extending to lower masses and redshift. As shown in Section 3.1, we tend to find larger relaxed fractions in low-mass and low-redshift samples. Finally, it is also possible that the *Planck* sample may be biased in the opposite direction of X-ray surveys, by preferentially selecting disturbed objects, but it is not possible to separate those effects with present data.

### 4.2 Comparison with previous SZ results

A first attempt to characterize the dynamical state of SZ-selected clusters has been performed by Song et al. (2012) for the first 720 deg$^2$ survey of the South Pole Telescope. They use the offset between the BCG and the SZ centroid as indicator of dynamical state and compare the distribution in their sample with the distribution of the BCG-X-ray peak offset for other X-ray-based samples, namely Lin & Mohr (2004) and Mann & Ebeling (2012). They report a good agreement between their observed distribution and the Lin & Mohr (2004) sample (41 per cent probability of consistency), while the agreement is not good with the Mann & Ebeling (2012) sample (0.46 per cent null-hypothesis probability). They justify this disagreement in terms of differences in the BCG selection procedure and decide to compare their results only with the more consistent Lin & Mohr (2004) sample, concluding that there is no compelling evidence that the dynamical state of SZ-selected clusters is different than in X-ray-selected clusters.

However, the number of objects where the difference in the BCG selection procedure between the Mann & Ebeling (2012) procedure and the SPT one may have led to a different measurement of the offset is very limited (2–3 clusters; Mann, private communication). These include cases where: (i) two or more elliptical galaxies with colours consistent with the clusters and similar magnitudes lie within the virial radius of the cluster; (ii) double clusters. The exclusion of the MACS sample from the comparison is thus not justified as this small number of objects may not have influenced the properties of the whole distribution. More importantly, we underline that the Mann & Ebeling (2012) sample is a well-defined X-ray-selected sample, while the Lin & Mohr (2004) is not X-ray-selected: it is an archival sample built from a collection of X-ray cluster catalogues with published temperature and with a redshift cut $z < 0.09$. Finally, the position of the SZ centroid does not necessarily coincide with the position of the X-ray peak and therefore the comparison of the SPT distribution with X-ray samples is not straightforward.

Another important result on the properties of clusters selected by SPT through the SZ effect has been published by McDonald et al. (2013), who analysed the *Chandra* observations of the highest S/N detections in the SPT survey. While the main objective of their paper is the evolution of the core properties with time, McDonald et al. (2013) also measure the fraction of CCs in their total sample and found it to be in the range of 10–40 per cent. While its exact value depends on the indicator and evolves with redshift, the fraction of CC is in any case smaller than the typical values observed in the X-ray-selected samples we considered. As discussed in Section 4.1, the CC fraction cannot be directly related to our relaxed fraction, as measured by our dynamical indicator. Nonetheless, the result in McDonald et al. (2013) provides an independent indirect suggestion of different selection effects between SZ and X-ray surveys.

Recently, Sehgal et al. (2013) showed that significant offsets between the BCG and the centre of the gas distribution induce an error in recovering the SZ signal with ACT of optically selected MaxBCG clusters. They estimate the $D_{\mathrm{X-BCG}}$ distribution for an X-ray-selected subsample of MaxBCG, but show it is not sufficient to explain the discrepancy between the *Planck*- and the ACT-recovered fluxes. However, the $D_{\mathrm{X-BCG}}$ distribution in X-ray-selected samples is likely biased towards relaxed objects. Thus, the offset distribution used in the analysis of Sehgal et al. (2013) may not be representative of the entire MaxBCG population and the correction of the ACT fluxes due to miscentring may be larger than estimated.

## 5 SUMMARY AND CONCLUSIONS

In this paper, we studied the dynamical state of a representative subsample of the catalogue of galaxy clusters observed by *Planck* with the SZ-effect (Planck Collaboration XXIX 2014). We have used as indicator of dynamical state the projected offset between the position of the X-ray peak and the position of the BCG, which is expected to be small for relaxed objects and larger for disturbed systems. By dividing our sample in redshift and mass bins, we find a suggestive indication (at 2.5–2.8$\sigma$) that high-mass and high-redshift subsamples host more disturbed objects than the low-mass and low-z samples. We compared the distributions of our indicator in the *Planck* sample with three X-ray-selected catalogues (HIFLUGCS, MACS and REXCESS) and found that the distributions are significantly different: the fraction of relaxed objects in our sample is significantly smaller ($>3\sigma$) with respect to the X-ray samples and the statistical test we applied to the $D_{\mathrm{X-BCG}}$ distributions return very small probabilities that the *Planck* and X-ray samples are drawn from the same parent distribution. We have shown that this difference is not due to the mass and redshift distributions, but is likely due to different selection effects affecting X-rays (the so-called CC bias) and, possibly, SZ surveys. Indeed, we confirm with our analysis the early impression that many *Planck* detected clusters are dynamically disturbed systems (Planck Collaboration IX 2011) and we provide the first observational indication that the SZ-selection is less biased towards relaxed objects than the X-ray selection.

An intrinsic limitation of the indicator used in our analysis is that it suffers from projection effects: if a merger is separating the BCG and the X-ray peak mainly along the line of sight, $D_{\mathrm{X-BCG}}$ would be underestimated with respect to the true physical offset. Consequently, a number of dynamically disturbed objects are mis-classified as relaxed and the fraction of relaxed objects measured with $D_{\mathrm{X-BCG}}$ in all samples is likely overestimated. This effect should be taken into account when comparing it to similar quantities obtained with other indicators, which do not suffer from projection effects. We tried to correct for this effect (as described in Appendix B) and we estimate the real fraction of relaxed objects in the *Planck* sample to be 45 per cent. However, even after this correction, $D_{\mathrm{X-BCG}}$ is still a dynamical indicator and the comparison of our relaxed fraction with the CC fraction obtained from thermodynamical indicators is not straightforward and requires several assumptions. A further limitation of our analysis is our estimate of the BCG from a heterogeneous set of literature information which may result in an underestimation of the measured offset for a few clusters (Section 2.3). This limitation does not affect only our sample but to a different extent also the MACS and REXCESS sample (Section 3.2).

Our work should be considered as a first step towards a description of the dynamical and thermodynamical state of *Planck* SZ-selected clusters. It will soon be possible to complement it and verify these results with several morphological indicators on X-ray images (centre shift, power ratios, concentration parameter) as well as thermodynamical quantities (central entropy and cooling time, entropy ratio) on similar representative subsamples of the *Planck* catalogue. These studies will allow us to firmly assess the fraction of CCs in *Planck* SZ-selected samples and compare them with the values derived from X-ray surveys and with predictions of simulations and thus establish the difference between SZ and X-ray-selected surveys.

## ACKNOWLEDGEMENTS

We thank the referee B. Maughan for a careful reading of the manuscript and W. Cui, T. Lauer, T. Reiprich, M. McDonald, N. Seghal, Z. Wen for sending us useful comments and bibliography. We thank H. Ebeling for providing the BCG coordinates of four MACS clusters. MR acknowledges useful discussions with A. Mann, J.B. Melin and S. Tunesi. FG acknowledges the financial contribution from contracts ASI-INAF I/037/12/0 and PRIN-INAF 2012 ‘A unique data set to address the most compelling open questions about X-ray clusters’. This research has made use of the NED, operated by the Jet Propulsion Laboratory, California Institute of Technology, under contract with the National Aeronautics and Space Administration.

## REFERENCES

Arnaud M., Pratt G. W., Piffaretti R., Böhringer H., Croston J. H., Pointecouteau E., 2010, A&A, 517, A92

Battaglia N., Bond J. R., Pfrommer C., Sievers J. L., 2012, ApJ, 758, 74

Beers T. C., Geller M. J., 1983, ApJ, 274, 491

Benson B. A. et al., 2013, ApJ, 763, 147

Bildfell C., Hoekstra H., Babul A., Mahdavi A., 2008, MNRAS, 389, 1637

Bleem L. E. et al., 2015, ApJS, 216, 27

Böhringer H. et al., 2007, A&A, 469, 363

Bonafede A., Intema H. T., Brüggen M., Girardi M., Nonino M., Kantharia N., van Weeren R. J., Röttgering H. J. A., 2014, ApJ, 785, 1

Boschin W., Girardi M., Barrena R., Nonino M., 2012, A&A, 540, A43

Brough S., Collins C. A., Burke D. J., Lynam P. D., Mann R. G., 2005, MNRAS, 364, 1354

Brough S., Couch W. J., Collins C. A., Jarrett T., Burke D. J., Mann R. G., 2008, MNRAS, 385, L103

Buote D. A., Tsai J. C., 1995, ApJ, 452, 522

Cavagnolo K. W., Donahue M., Voit G. M., Sun M., 2009, ApJS, 182, 12

Coziol R., Andernach H., Caretta C. A., Alamo-Martínez K. A., Tago E., 2009, AJ, 137, 4795

Crawford C. S., Edge A. C., Fabian A. C., Allen S. W., Bohringer H., Ebeling H., McMahon R. G., Voges W., 1995, MNRAS, 274, 75

Crawford C. S., Allen S. W., Ebeling H., Edge A. C., Fabian A. C., 1999, MNRAS, 306, 857

Cui W. et al., 2016, MNRAS, 456, 2566

Ebeling H., Edge A. C., Henry J. P., 2001, ApJ, 553, 668

Ebeling H., Ma C. J., Kneib J.-P., Jullo E., Courtney N. J. D., Barrett E., Edge A. C., Le Borgne J.-F., 2009, MNRAS, 395, 1213

Eckert D., Molendi S., Paltani S., 2011, A&A, 526, A79

Edge A. C., 1991, MNRAS, 250, 103

Edge A. C., Stewart G. C., 1991, MNRAS, 252, 414

Evans I. N. et al., 2010, ApJS, 189, 37

Feigelson E., Babu G., 2012, Modern Statistical Methods for Astronomy: With R Applications. Cambridge Univ. Press, Cambridge, (available at: https://books.google.it/books?id=M6O1yxpvf2gC)

Gradshteyn I. S., Ryzhik I. M., 2007, Table of Integrals, Series, and Products, seventh edn. Elsevier/Academic Press, Amsterdam

Guzzo L. et al., 2009, A&A, 499, 357

Haarsma D. B. et al., 2010, ApJ, 713, 1037

Hashimoto Y., Henry J. P., Boehringer H., 2014, MNRAS, 440, 588

Hasselfield M. et al., 2013, J. Cosmol. Astropart. Phys., 7, 8

Hoffer A. S., Donahue M., Hicks A., Barthelemy R. S., 2012, ApJS, 199, 23

Hudson D. S., Mittal R., Reiprich T. H., Nulsen P. E. J., Andernach H., Sarazin C. L., 2010, A&A, 513, A37

Jones C., Forman W., 1984, ApJ, 276, 38

Jones C., Forman W., 1999, ApJ, 511, 65

Katayama H., Hayashida K., Takahara F., Fujita Y., 2003, ApJ, 585, 687

Koester B. P. et al., 2007, ApJ, 660, 239

Krause E., Pierpaoli E., Dolag K., Borgani S., 2012, MNRAS, 419, 1766

Lauer T. R., Postman M., Strauss M. A., Graves G. J., Chisari N. E., 2014, ApJ, 797, 82

Leccardi A., Rossetti M., Molendi S., 2010, A&A, 510, A82

Lin H. W., McDonald M., Benson B., Miller E., 2015, ApJ, 802, 34

Lin Y.-T., Mohr J. J., 2004, ApJ, 617, 879

McDonald M., Benson B. A., Vikhlinin A., Stalder B., Bleem L. E., de Haan T., Lin H. W., Aird K. A., 2013, ApJ, 774, 23

McNamara B. R. et al., 2006, ApJ, 648, 164

Malumuth E. M., Kriss G. A., Dixon W. V. D., Ferguson H. C., Ritchie C., 1992, AJ, 104, 495

Mann A. W., Ebeling H., 2012, MNRAS, 420, 2120

Menanteau F. et al., 2010, ApJ, 723, 1523

Motl P. M., Hallman E. J., Burns J. O., Norman M. L., 2005, ApJ, 623, L63

Oegerle W. R., Hill J. M., 2001, AJ, 122, 2858

Owers M. S., Nulsen P. E. J., Couch W. J., Markevitch M., 2009, ApJ, 704, 1349

Owers M. S., Randall S. W., Nulsen P. E. J., Couch W. J., David L. P., Kempner J. C., 2011, ApJ, 728, 27

Patel P., Maddox S., Pearce F. R., Aragón-Salamanca A., Conway E., 2006, MNRAS, 370, 851

Peres C. B., Fabian A. C., Edge A. C., Allen S. W., Johnstone R. M., White D. A., 1998, MNRAS, 298, 416

Pipino A., Pierpaoli E., 2010, MNRAS, 404, 1603
Planck Collaboration IX, 2011, A&A, 536, A9
Planck Collaboration XX, 2014, A&A, 571, A20
Planck Collaboration XXIX, 2014, A&A, 571, A29
Planck Collaboration XXIV, 2015, A&A, preprint (arXiv:1502.01597)
Planck Collaboration XXVII, 2015, A&A, preprint (arXiv:1502.01598)
Planck Collaboration XXXII, 2015, A&A, 581, A14
Poole G. B., Fardal M. A., Babul A., McCarthy I. G., Quinn T., Wadsley J., 2006, MNRAS, 373, 881
Postman M., Lauer T. R., 1995, ApJ, 440, 28
R Core Team 2015, R: A Language and Environment for Statistical Computing. R Foundation for Statistical Computing, Vienna, (available at: https://www.R-project.org)
Rawle T. D. et al., 2012, ApJ, 747, 29
Reiprich T. H., Böhringer H., 2002, ApJ, 567, 716
Rykoff E. S. et al., 2014, ApJ, 785, 104
Sanderson A. J. R., Edge A. C., Smith G. P., 2009, MNRAS, 398, 1698
Santos J. S., Rosati P., Tozzi P., Böhringer H., Ettori S., Bignamini A., 2008, A&A, 483, 35
Sehgal N. et al., 2013, ApJ, 767, 38
Skibba R. A., Macciò A. V., 2011, MNRAS, 416, 2388
Song J. et al., 2012, ApJ, 761, 22
Stanford S. A., Eisenhardt P. R., Dickinson M., Holden B. P., De Propris R., 2002, ApJS, 142, 153
Story K. et al., 2011, ApJ, 735, L36
Stott J. P., Edge A. C., Smith G. P., Swinbank A. M., Ebeling H., 2008, MNRAS, 384, 1502
Stott J. P. et al., 2012, MNRAS, 422, 2213
Sun M., 2009, ApJ, 704, 1586
Sunyaev R. A., Zeldovich Y. B., 1970, Comments Astrophys. Space Phys., 2, 66
Sunyaev R. A., Zeldovich Y. B., 1972, Comments Astrophys. Space Phys., 4, 173
Taylor M. B., 2005, in Shopbell P., Britton M., Ebert R., eds, ASP Conf. Ser. Vol. 347, Astronomical Data Analysis Software and Systems XIV. Astron. Soc. Pac., San Francisco, p. 29
Valtchanov I., Murphy T., Pierre M., Hunstead R., Lémonon L., 2002, A&A, 392, 795
van den Bosch F. C., Weinmann S. M., Yang X., Mo H. J., Li C., Jing Y. P., 2005, MNRAS, 361, 1203
van Weeren R. J. et al., 2013, ApJ, 769, 101
Varela J. et al., 2009, A&A, 497, 667
Vikhlinin A. et al., 2009, ApJ, 692, 1060
Wall J., Jenkins C., 2003, Practical Statistics for Astronomers. Cambridge Observing Handbooks for Research Astronomers, Cambridge Univ. Press, Cambridge, (available at: https://books.google.it/books?id=ekyupqnDFzMC)
Wen Z. L., Han J. L., Liu F. S., 2012, ApJS, 199, 34
Williamson R. et al., 2011, ApJ, 738, 139
Zhang Y.-Y., Andernach H., Caretta C. A., Reiprich T. H., Böhringer H., Puchwein E., Sijacki D., Girardi M., 2011, A&A, 526, A105

## SUPPORTING INFORMATION

Additional Supporting Information may be found in the online version of this article:

**Table 1.** Properties of the clusters in our sample.
**Appendix A.** Notes on individual objects.
**Appendix B.** Impact of projection effects.
(http://www.mnras.oxfordjournals.org/lookup/suppl/doi:10.1093/mnras/stw265/-/DC1).

This paper has been typeset from a TEX/LATEX file prepared by the author.